ACS chemical biology

Letters

pubs.acs.org/acschemicalbiology

Evidence for Age-Dependent *in Vivo* Conformational Rearrangement within Aβ Amyloid Deposits

Sofie Nyström,[†] Katarzyna M. Psonka-Antonczyk,[‡] Pål Gunnar Ellingsen,[‡] Leif B. G. Johansson,[†] Nina Reitan,[‡] Susann Handrick,[§] Stefan Prokop,[§] Frank L. Heppner,[§] Bettina M. Wegenast-Braun,[∥,⊥] Mathias Jucker,[∥,⊥] Mikael Lindgren,[†,‡] Bjørn Torger Stokke,[‡] Per Hammarström,[†,*] and K. Peter R. Nilsson[†]

[†]IFM-Department of Chemistry, Linköping University, Linköping, Sweden

[‡]Department of Physics, The Norwegian University of Science and Technology, Trondheim, Norway

[§]Department of Neuropathology, Charité, Universitätsmedizin Berlin, Berlin, Germany

[∥]German Center for Neurodegenerative Diseases, Tübingen, Germany

[⊥]Department of Cellular Neurology, Hertie-Institute for Clinical Brain Research, University of Tübingen, Tübingen, Germany

Supporting Information

ABSTRACT: Deposition of aggregated Aβ peptide in the brain is one of the major hallmarks of Alzheimer's disease. Using a combination of two structurally different, but related, hypersensitive fluorescent amyloid markers, LCOs, reporting on separate ultrastructural elements, we show that conformational rearrangement occurs within Aβ plaques of transgenic mouse models as the animals age. This important mechanistic insight should aid the design and evaluation of experiments currently using plaque load as readout.

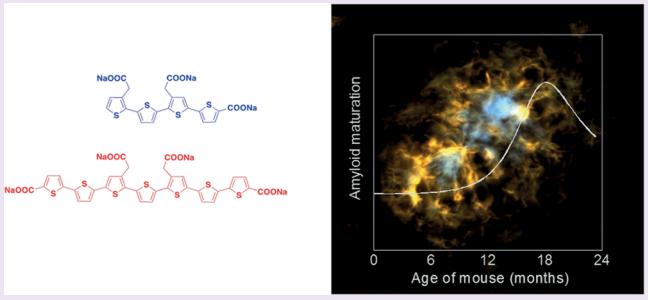

Formation of amyloid plaques from Aβ peptide is one major pathologic hallmark of Alzheimer's disease (AD)[1] and, as such, has been widely studied. Nevertheless, the connection between Aβ plaque formation and clinical disease is not fully understood, but Aβ deposition is projected to precede neurodegeneration.[2] Recent studies of biomarkers in familial AD carriers show that neuronal damage and Aβ deposition precedes cognitive impairment by 15 years.[3] Clinical cognitive impairment starts to appear at the same time as acceleration of plaque deposition decreases.[3] Nonetheless, the clinical progression toward dementia relentlessly advances after this stage implicating possible uncharted evolvement of amyloid pathology during aging. It is not known how the brain resists Aβ-toxicity during the lengthy phase of deposition. The observations from biomarkers and clinical symptoms may suggest that deposition and toxicity occurs in two distinct temporal phases[4] as shown for prion diseases.[5] Although a large number of transgenic animal models of AD are available, little is known about late stage Aβ plaque maturation. There have been reports of successful imaging of plaque growth in mouse models imaged *in vivo* over time[6−9] focusing on mice younger than 12 months. Hefendehl et al.[6] monitored plaque growth in APP/PS1 (an early onset AD mouse model)[10] mice between 3.7 and 10 months of age and detected appearance of new plaques. It was found that the formation of new plaques was most prominent in young mice, while from approximately 8 months of age on, almost no formation of new plaques was observed while existing plaques appeared to grow. In general, few studies of amyloid plaques in APP/PS1 mice involve mice older than 12 months.

Recently, luminescent conjugated poly- and oligothiophenes (LCPs and LCOs) have proven suitable to report on conformational differences in amyloid structure *in vitro* and *ex vivo*.[11−14] Herein, it was shown that the tetrameric oligothiophene qFTAA (quadro-formylthiophene acetic acid) (Figure 1a) responds to mature Aβ amyloid fibrils, whereas the heptameric oligo-thiopene hFTAA (hepta-formylthiophene acetic acid) (Figure 1a) in addition to staining mature amyloid fibrils also responds to early prefibrillar states of Aβ formed during the *in vitro* fibril formation process.[12] Importantly, fluorescence from the two LCOs can be easily discriminated by virtue of their spectra (Figure 1b).

This should allow simultaneous staining followed by hyperspectral evaluation of fluorescence signatures. Side chain packing, and possibly secondary structure,[15] within prefibrillar Aβ aggregates and mature fibrous Aβ fibrils are by default different. The conformational change from prefibrillar to mature amyloid fibril can be viewed as a supermolecular version of intermediately folded molten globules and native

Received: January 17, 2013
Accepted: March 24, 2013
Published: March 25, 2013

   dx.doi.org/10.1021/cb4000376 | *ACS Chem. Biol.* 2013, 8, 1128−1133

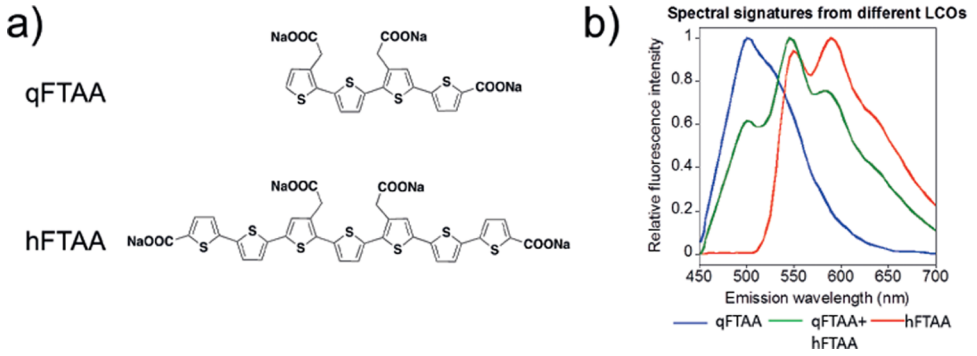

Figure 1. Chemical structures and fluorescence profiles of qFTAA and hFTAA (a). (b) Normalized spectra from amyloid plaques in tissue stained with either qFTAA (blue) or hFTAA (red), respectively. The mathematical sum of the two separate spectra is represented in green.

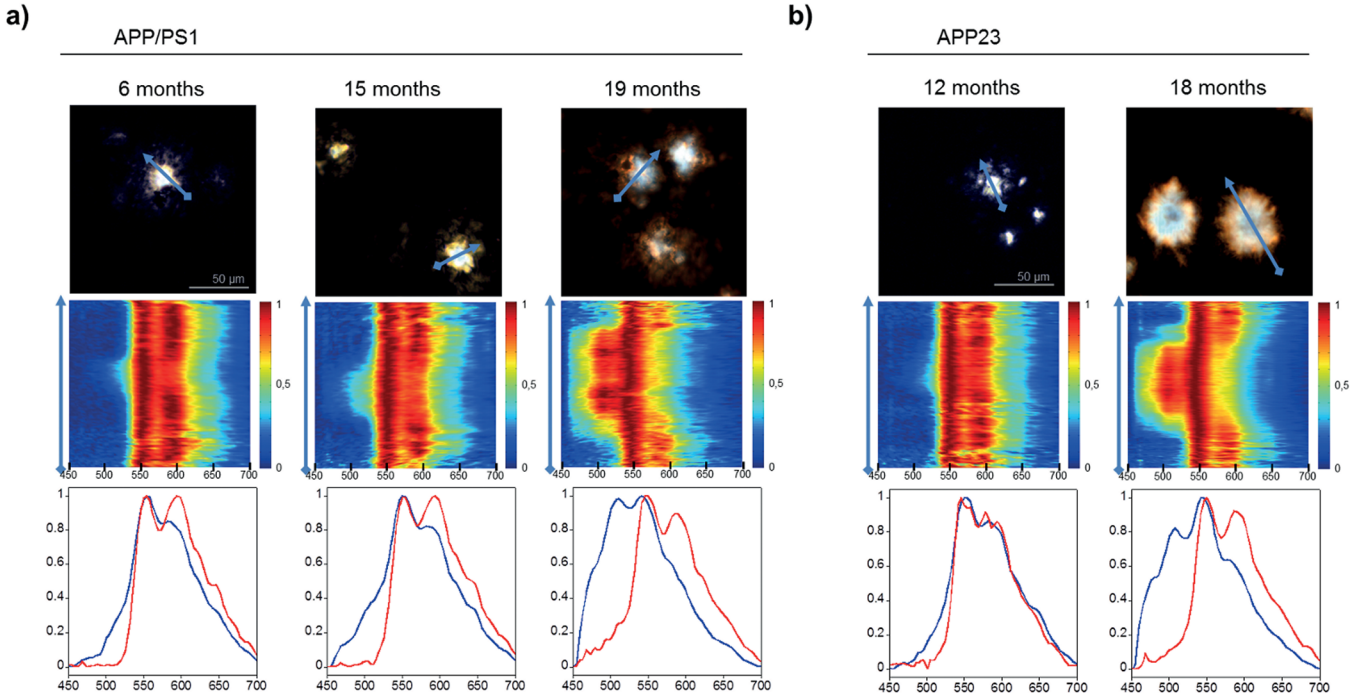

Figure 2. Fluorescence images and spectral analysis of brain cryosections stained with premixed qFTAA and hFTAA. (a) APP/PS1 mice of different ages as indicated in the figure. (b) APP23 mice of different ages as indicated in the figure. Analysis of individual plaques using hyperspectral imaging revealed that the center of the plaque displayed a relative increase in qFTAA fluorescence as the mice aged. Normalized spectra from cross-sections of single plaque are displayed as heat maps, reflecting low to high intensities ranging from blue to red. Normalized spectra from the center (blue) and periphery (red) are displayed below each heat map.

states in protein folding reactions. In the current study, we used a combination of qFTAA and hFTAA to address conformational differences within Aβ plaque as a function of animal age. To test this hypothesis, we used cohorts of transgenic mice with a broad age span and fluorescence microspectroscopy for histochemical analysis of Aβ deposits.

Brains from APP/PS1 mice aged 6, 15, and 19 months were stained with a mixture of qFTAA and hFTAA. High magnification studies of individual plaques using hyperspectral fluorescence imaging suggested distinct staining patterns using qFTAA and hFTAA dependent on the age of the mice and region within individual plaques (Figure 2a). In young mice, only hFTAA bound to the plaques, while in older mice, the amount of qFTAA fluorescence from the core of the plaque increased, whereas the rim of the plaque still displayed only hFTAA fluorescence. A similar profile was observed for APP23 mice aged 12 or 18 months (Figure 2b), an AD mouse model with later onset of amyloid pathology than APP/PS1.[16] The notion that amyloid plaques are structurally different as one travels outward from the center has been reported previously in humans[17] and transgenic mice.[13]

To further analyze the temporal spectral variation, sections from APP/PS1 mice aged 5−23 months (n = 19) were stained. The spectral contribution of the respective LCO was quantified by the ratio of the fluorescence intensity at 500 nm (I_{500}) reflecting qFTAA and 540 nm (I_{540}) reflecting hFTAA. Spectra from the center of 45 randomly selected plaques were collected from each mouse. Plotting I_{500}/I_{540} versus age generated a kinetic trace reflecting plaque maturation (Figure 3a). The spectral analyses revealed a more prominent contribution from qFTAA, starting at about 11 months with a peak at 18−19 months. At 20 months, I_{500}/I_{540} decreased suggesting a relative increase of hFTAA staining within the plaque cores (Figure 3a). Dividing the age trajectory raw data into age groups (4−11,

dx.doi.org/10.1021/cb4000376 | ACS Chem. Biol. 2013, 8, 1128−1133

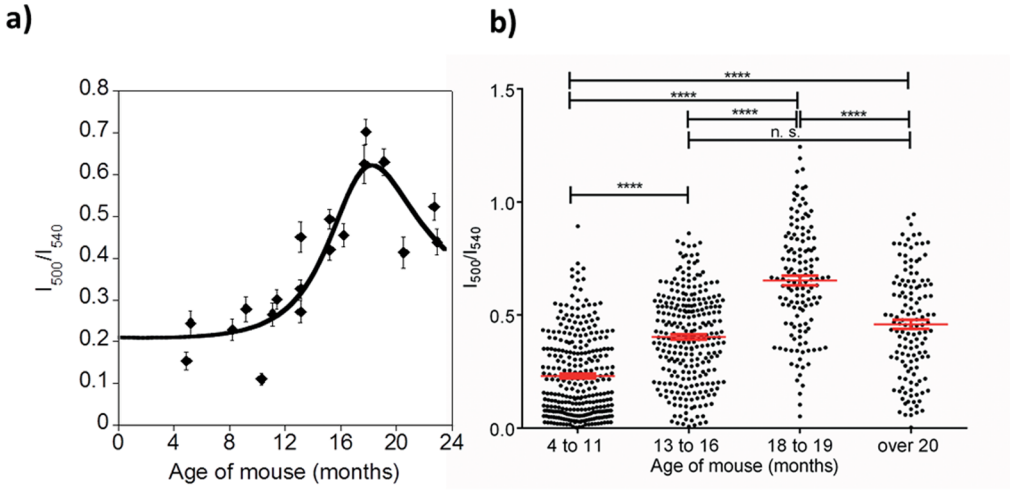

c)

Representation of plaque morphology												
Age of mouse	6 months		12 months			18 months			22 months			
Fibril types observed	immature		immature	maturating		maturating	mature		immature	maturating	mature	
qFTAA	-		-	(+)			(+)	+	-	(+)	+	
hFTAA	+		+	+			+	+	+	+	+	

Figure 3. Age-dependent variation of plaque staining in APP/PS1 mice when stained simultaneously with qFTAA and hFTAA. (a) Diagram showing the ratio of intensity of the emitted light at 500 and 540 nm, I_{500}/I_{540}, versus age. The fluorescence intensity at 500 nm (I_{500}) reflects qFTAA emission, whereas the intensity at 540 nm (I_{540}) reflects hFTAA emission. Spectra from the center of 45 randomly selected plaques from each mouse (855 plaques in total) were subjected to ratiomeric calculation to disclose spectral shift reflecting increase in qFTAA binding as a function of mouse age. Error bars represent SEM. (b) Statistical analysis of different age groups using ANOVA test. **** = $p < 0.0001$ for pairwise comparison of consecutive age groups; n.s. = nonsignificant. (c) Graphical representations of observed plaque morphologies and Aβ fibril types discriminated by fluorescence spectra; hFTAA positive fibrils represented in red and qFTAA positive fibrils represented in blue. Fluorescence signal from qFTAA and hFTAA: + = positive; (+) = weak; − = negative. The proposed model for plaque formation and maturation is shown in Supplementary Video 1.

13−16, 18−19, and >20 months) and subjecting the groups to statistical analyses (one-way ANOVA and *t* test), it showed that the differences are highly significant between the different age transitions (Figure 3b). Confirming analysis of the data was done using a custom developed algorithm[18] for determining the correlation coefficient with respect to the pure qFTAA in comparison to hFTAA spectrum in the center of the plaque (Supplementary Figure 1). It was also striking how amyloid fibril morphology changed over time. Simplified graphical models of the observed fibril types and a proposed mechanism for plaque maturation as a function of time are displayed in Figure 3c and Supplementary Video 1.

Corresponding reference samples of APP/PS1 stained by Congo red (Supplementary Figure 2) demonstrated that strong qFTAA staining essentially coincided with Congo red staining, whereas the peripheral plaque coronas were Congo red negative but readily stained by hFTAA. Hence, combined LCO staining revealed more extensive amyloid pathology than Congo red. In addition, immunohistochemistry confirmed that LCO staining coincides with the presence of Aβ deposition (Supplementary Figure 2) as previously shown.[19]

The observed staining differences within plaque deposits prompted further investigation of the difference in staining propensity between different probes within different regions of single plaque. Hence, analogous sections from one 18 months old APP/PS1 mouse and one 18 months old APP23 mouse were stained with ThT, qFTAA, and hFTAA, respectively. This comparison clearly demonstrated the different staining capabilities of the different probes (Supplementary Figure 3a,b). In APP/PS1 mice, qFTAA stained essentially the same structures as ThT, although intensity using ThT was much weaker, despite 5−10-fold higher probe concentration and 10-fold increased exposure time during imaging. In addition to plaque cores, the hFTAA staining revealed large areas of diffuse protein aggregates surrounding the plaque core as well as small squiggly fibrils between plaques as described in Figure 2a and corroborating analysis of morphologies in Supplementary Figure 3a. The same conclusions were drawn from comparisons using the thioflavin T derivative 6-CN-BTA-1 (CN-PiB), a fluorescent analogue to the clinically used PET ligand PiB[20] and hFTAA in a stepwise costaining study. CN-PiB and hFTAA colocalize in the core, and hFTAA, in addition, shows peripheral staining of plaque. Stepwise costaining with qFTAA and CN-PiB demonstrated that corresponding areas, i.e., the center of the plaque, are stained by both probes (Supplementary Figure 4.). In APP23 mice, the hFTAA stained rims surrounding a qFTAA stained center of individual plaques were smaller and followed the geometry of the plaque cores. Amyloid deposits within the vasculature were dominated by hFTAA, whereas the regions only stained with qFTAA were smaller and fewer.

To corroborate that the differentiated staining pattern could be attributed to conformational rearrangements during maturation of Aβ fibril structures, *in situ* and *ex situ* kinetic

dx.doi.org/10.1021/cb4000376 | *ACS Chem. Biol.* 2013, 8, 1128−1133

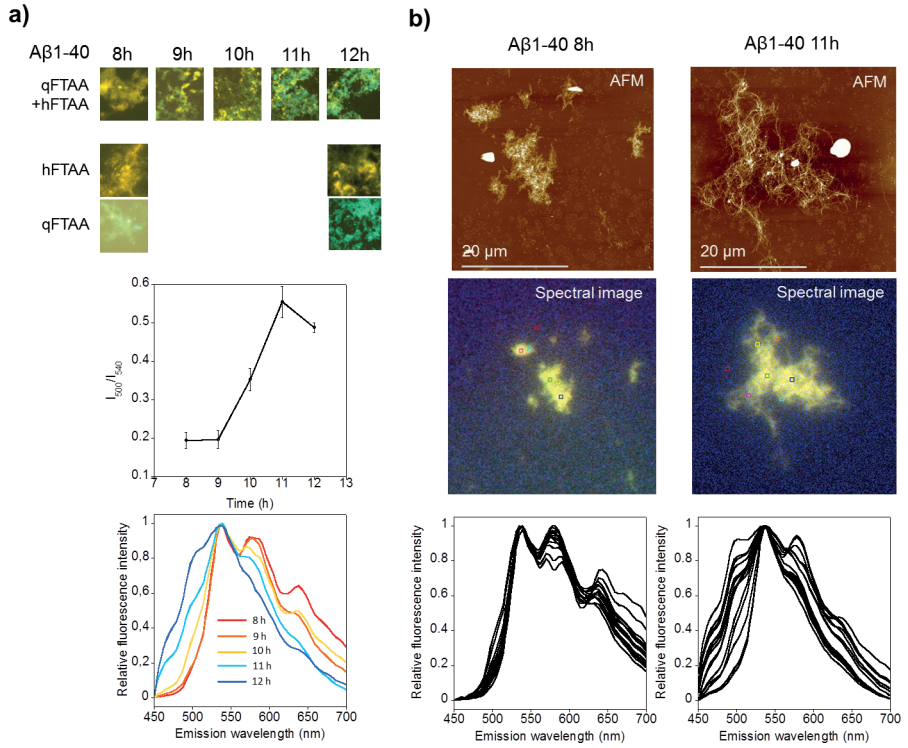

Figure 4. Fibrillation and staining of recombinant Aβ1−40. (a) *In vitro* formed fibrils of Aβ1−40 were collected at different time points and were stained with a mixture of qFTAA and hFTAA. The sedimented aggregates were placed on microscope glass and imaged using hyperspectral imaging. The ratio between peak intensities at 500 and 540 nm was plotted against time. The kinetics disclose an increase in qFTAA fluorescence over time. (b) Samples from time points dominated by hFTAA and qFTAA fluorescence, respectively, were selected for AFM analysis. Fibrils at 8 h showed strong hFTAA spectra and displayed disordered bundles of short protofibrils, whereas fibrils at 11 h with strong qFTAA fluorescence contained long slender mature fibrils.

fibrillation experiments of Aβ1−40 (Figure 4) and Aβ1−42 (Supplementary Figure 5) were performed. Aggregates that formed early (<10 h) extracted from Aβ1−40 fibrillation reactions were solely stained by hFTAA. The aggregates started to display qFTAA fluorescence >10 h *ex situ*. Separate staining with either qFTAA or hFTAA confirmed that qFTAA fluorescence was weak at early time points (Figure 4a).

The Aβ1−42 samples displayed a similar staining pattern as Aβ1−40, but the qFTAA fluorescence did not reach the same intensity as for Aβ1−40 fibrils. ThT fluorescence was shown to correlate well to the kinetics of qFTAA fluorescence, whereas hFTAA responded during the qFTAA and ThT silent lagphase in kinetic fibrillation assays (Supplementary Figure 5).[12]

Atomic force microscopy (AFM) was employed to decipher ultrastructural differences within fibrillar assemblies giving rise to the diverse staining patterns. Samples from early and late time points of an Aβ1−40 fibrillation reaction were imaged using AFM colocalized with hyperspectral imaging. The images revealed a larger extent of mature filamentous fibers in the late time points showing strong qFTAA fluorescence (Figure 4b). The early time points, displaying only hFTAA fluorescence, reveal bundles constituted of markedly shorter protofibrillar species (Figure 4b).

In the current study, we have monitored APP/PS1 mice at different ages between 5 to 23 months *ex vivo*. Our focus has not been to assess on the quantity of plaques but rather the Aβ conformation within individual plaques. It is interesting, however, to note that, as the quantity of core plaques appears to reach a plateau, the staining pattern of individual plaques starts to change. Plaques in mice younger than 10 months are almost exclusively stained by hFTAA (Figure 3), similar to early immature fibrils of recombinant Aβ (Figure 4a,b). As APP/PS1 mice grow older, the core of the plaques appears to rearrange, and its ability to bind qFTAA increases in the same manner as mature filamentous recombinant Aβ fibrils do *in vitro*. The ratiomeric transition curve reaches a maximum at around 18 months (Figure 3a), and after this time point, the I_{500}/I_{540} ratio reflects either an increase of hFTAA binding or a decrease of qFTAA binding to the plaques. Microscopic assessment revealed an increase in diffuse hFTAA stainable deposits between the core plaques at 23 months that were stained by 6E10 antibody, but not by Congo red or qFTAA (Supplementary Figure 2). Since the imaged plaques were randomly selected, this likely reflects the initiation of a second wave of *de novo* formation of core plaques that has not been reported previously, most likely because the experiments have been terminated and/or because conventional amyloid dyes do not detect these structures. This step could hypothetically mimic development of spreading amyloid pathology in human AD. A similar conclusion was derived from oligomer specific antibody studies of 3xTg-AD mice, showing two separate temporal waves of oligomer formation (at 6 mo and >15 mo).[21] Amyloid maturation likely correlates to pathophysiological phenotypes in APP/PS1 mice. Young (5 mo) APP/PS1 mice do not show major change in behavior, whereas decreased performance in Barnes maze, novel object recognition, and contextual fear conditioning paradigm appear in approximately 8 month old mice.[10,22] Hippocampal synaptic plasticity measured by long-term potentiation is unaffected in young mice (<5 mo) but is significantly reduced at 8 months and even more so at 15

dx.doi.org/10.1021/cb4000376 | *ACS Chem. Biol.* 2013, 8, 1128−1133

months of age.[23] Recent data showed that dendritic spine loss in APP/PS1 mice near amyloid plaque appear constant in young (3 mo) and aged mice (18 mo).[24] Importantly, only in young mice there is nascent plaque formation and significant plaque growth; nevertheless, the dendritic spine loss persists near amyloid plaque in aged mice. This suggests a correlation to our hypothesis of ongoing remodeling within and around Aβ plaque at 18 months of age. We have also analyzed APP23 mice (n = 4) at ages 12 and 18 months, and they display an identical type of maturation profile of the plaque core (Figure 2b), suggesting unexpectedly that amyloid maturation of the core as a function of mouse age appears to be independent of onset of Aβ pathology. APP23 mice generate a higher Aβ40/Aβ42 ratio than APP/PS1 mice,[10,14,16] and this, in the context of weak qFTAA staining of recAβ1−42 (Supplementary Figure 5a,b), could explain why qFTAA staining is weaker in APP/PS1 plaques, and the surrounding rim of hFTAA stained material is larger and more predominant in the APP/PS1 mice. An extended study of APP23 mice (n = 27) of ages 6, 12, 18, 25, and 30 months has been performed (to be published elsewhere), which confirms the maturation transition between 12 and 18 months as shown in Figure 2b.

By the rather straightforward approach of combining two hypersensitive small molecule reporter dyes, we discovered differences in plaque morphology in APP/PS1 mice at different ages. The chemical structure of the shorter qFTAA (Figure 1a) as well as the ultrastructural studies shown in this letter suggest that this probe requires a similar mature ordered fibril structure as that of ThT, Congo red, and CN-PiB, to display elevated fluorescence. The longer hFTAA (Figure 1a), however, evidently has more promiscuous preferences and reports on more disordered structures as well as on filamentous amyloid and mature fibrils. The discrepancies in response propensity of the two probes enabled microscopic assessment of temporal dynamic formation and maturation of Aβ amyloid as summarized in Figure 3c and Supplementary Video 1. Importantly, we observed two hitherto unreported transitions, past the age of 12 months, in plaque staining patterns. Our data strongly suggest that this finding reflects conformational rearrangements within amyloid deposits at old age. *In vitro* fibrillation kinetic data of pure recombinant Aβ corroborate that this transition is due to intrinsic Aβ fibril maturation without the need to invoke external influences such as glycosaminoglycan (GAG), serum amyloid P component (SAP), apolipoprotein E (ApoE), or microglial metabolism. To our knowledge, this is the most direct evidence provided for Aβ conformational maturation within and around Aβ plaque as a function of mouse age. Till date, plaque load has been one dominating readout in the evaluation of therapeutic intervention,[25] genotype,[26] and pathological seeding[27] in transgenic mice. Our novel approach for evaluation of Aβ pathology will open up for experiments linking structure to gain-of-toxic function for assessment of inert and neurotoxic Aβ aggregates or strains in AD.[28] Temporal experiments may also separate the hypothetical conformations of Aβ misfolding catalysts ($A\beta^{Cat}$) from toxic Aβ ($A\beta^{Tox}$) forms leaking from plaques.[29] We advocate that this technology should be used to stratify time windows for pathological and prognostic evaluations in preventive and therapeutic interventions in experiments using transgenic mice.

METHODS

A brief description of the methods used follows below. See Supporting Information for a complete methods section.

Staining of Tissue. qFTAA and hFTAA were synthesized as described previously.[12] The fluorescent probes were diluted to the following staining concentrations: 3.6 μM qFTAA, 2.4 μM hFTAA, (or 2.4 μM qFTAA and 0.77 μM hFTAA for simultaneous staining), 5 μM CN-PiB, 20 μM ThT, and 30 μg mL^{-1} Congo red. Cryosections from fresh frozen tissue was fixed in ethanol and rewetted in PBS prior to 30 min of staining.

For antibody labeling, 6E10 antibody diluted 1:100 in block solution and incubated overnight at 4 °C, where secondary antibody (Alexa Fluoro 488) was added.

Kinetics of Recombinant Aβ Fibrillation. Lyophilized recombinant Aβ1−40 and Aβ1−42 (rPeptide) was resuspended in 2 mM NaOH and diluted to 10 μM assay solution in PBS, pH 7.4, immediately prior to use.

Fluorescence Microscopy. Hyperspectral imaging of recombinant fibrils and tissue sections was performed using a Leica DM6000 B fluorescence microscope (Leica) equipped with a SpectraCube module (Applied Spectral Imaging). Forty-five plaques from each animal were analyzed by collecting spectra from the center of each plaque and calculating the ratio of the fluorescence intensities at 500 and 540 nm.

Atomic Force Microscopy (AFM). Recombinant Aβ fibrils were mounted on mica surface and imaged with AFM in air.

ASSOCIATED CONTENT

Supporting Information

Details regarding methods together with supporting figures and an animation describing the growth and maturation of an amyloid plaque. This material is available free of charge via the Internet at http://pubs.acs.org.

AUTHOR INFORMATION

Corresponding Author

*(P.H.) Phone: +46 13 285690. Fax: +46 13 281399.

Author Contributions

S.N., P.H., and K.P.R.N. designed the study; F.L.H., M.J., M.L., K.P.R.N., and P.H. initiated the project; S.N., K.M.P.A., L.B.G.J., and K.P.R.N. performed experiments; S.N., P.H., P.G.E., N.R., B.T.S., and M.L. analyzed data; S.H., S.P., F.L.H., B.M.W.B., and M.J. provided mice; S.N. and P.H. wrote the manuscript with the assistance from all authors.

Notes

The authors declare no competing financial interest.

ACKNOWLEDGMENTS

We thank C. Sluszny and D. Sjölander for helpful discussions and H. Levine III, B. Ciliax, and F. Zeng for providing CN-PiB. Brain tissue from APP23 mice was generously provided by M. Staufenbiel. This work was supported by the EU-FP7 Health Programme Project LUPAS (to B.M.W.B., F.L.H., M.J., M.L., N.R., P.G.E., P.H., K.P.R.N., S.H., S.N., and S.P.), the Swedish Alzheimer Foundation (to S.N.), the Swedish Research Council (to P.H.), Knut and Alice Wallenberg Foundation (to P.H. and K.P.R.N.), the Swedish Foundation for Strategic Research (to P.H. and K.P.R.N.), the European Research Council (ERC starting grant; Project MUMID) (to K.P.R.N.), the Norwegian Research Council (contract 183338/S10, to K.M.P.A. and B.T.S.), and a donation from Georg and Astrid Olsson (to P.H., K.P.R.N., and S.N.). P.H. is a Swedish Royal Academy of Science Research fellow sponsored by a grant from the Knut and Alice Wallenberg Foundation.

REFERENCES

(1) Hardy, J. A., and Higgins, G. A. (1992) Alzheimer's disease: the amyloid cascade hypothesis. *Science 256*, 184−185.

(2) Jack, C. R., Jr., Knopman, D. S., Jagust, W. J., Shaw, L. M., Aisen, P. S., Weiner, M. W., Petersen, R. C., and Trojanowski, J. Q. (2010) Hypothetical model of dynamic biomarkers of the Alzheimer's pathological cascade. *Lancet Neurol. 9*, 119−128.

(3) Bateman, R. J., Xiong, C., Benzinger, T. L., Fagan, A. M., Goate, A., Fox, N. C., Marcus, D. S., Cairns, N. J., Xie, X., Blazey, T. M., Holtzman, D. M., Santacruz, A., Buckles, V., Oliver, A., Moulder, K., Aisen, P. S., Ghetti, B., Klunk, W. E., McDade, E., Martins, R. N., Masters, C. L., Mayeux, R., Ringman, J. M., Rossor, M. N., Schofield, P. R., Sperling, R. A., Salloway, S., and Morris, J. C. (2012) Clinical and biomarker changes in dominantly inherited Alzheimer's disease. *N. Engl. J. Med. 367*, 795−804.

(4) Zetterberg, H., and Hammarstrom, P. (2012) Power tools for Alzheimer's disease: an electrochemical preamp for Abeta. *J. Neurochem. 122*, 231−232.

(5) Sandberg, M. K., Al-Doujaily, H., Sharps, B., Clarke, A. R., and Collinge, J. (2011) Prion propagation and toxicity *in vivo* occur in two distinct mechanistic phases. *Nature 470*, 540−542.

(6) Hefendehl, J. K., Wegenast-Braun, B. M., Liebig, C., Eicke, D., Milford, D., Calhoun, M. E., Kohsaka, S., Eichner, M., and Jucker, M. (2011) Long-term *in vivo* imaging of beta-amyloid plaque appearance and growth in a mouse model of cerebral beta-amyloidosis. *J. Neurosci. 31*, 624−629.

(7) Bolmont, T., Haiss, F., Eicke, D., Radde, R., Mathis, C. A., Klunk, W. E., Kohsaka, S., Jucker, M., and Calhoun, M. E. (2008) Dynamics of the microglial/amyloid interaction indicate a role in plaque maintenance. *J. Neurosci. 28*, 4283−4292.

(8) Meyer-Luehmann, M., Spires-Jones, T. L., Prada, C., Garcia-Alloza, M., de Calignon, A., Rozkalne, A., Koenigsknecht-Talboo, J., Holtzman, D. M., Bacskai, B. J., and Hyman, B. T. (2008) Rapid appearance and local toxicity of amyloid-beta plaques in a mouse model of Alzheimer's disease. *Nature 451*, 720−724.

(9) Yan, P., Bero, A. W., Cirrito, J. R., Xiao, Q., Hu, X., Wang, Y., Gonzales, E., Holtzman, D. M., and Lee, J. M. (2009) Characterizing the appearance and growth of amyloid plaques in APP/PS1 mice. *J. Neurosci. 29*, 10706−10714.

(10) Radde, R., Bolmont, T., Kaeser, S. A., Coomaraswamy, J., Lindau, D., Stoltze, L., Calhoun, M. E., Jaggi, F., Wolburg, H., Gengler, S., Haass, C., Ghetti, B., Czech, C., Holscher, C., Mathews, P. M., and Jucker, M. (2006) Abeta42-driven cerebral amyloidosis in transgenic mice reveals early and robust pathology. *EMBO Rep. 7*, 940−946.

(11) Hammarstrom, P., Simon, R., Nystrom, S., Konradsson, P., Aslund, A., and Nilsson, K. P. (2010) A fluorescent pentameric thiophene derivative detects *in vitro*-formed prefibrillar protein aggregates. *Biochemistry 49*, 6838−6845.

(12) Klingstedt, T., Aslund, A., Simon, R. A., Johansson, L. B., Mason, J. J., Nystrom, S., Hammarstrom, P., and Nilsson, K. P. (2011) Synthesis of a library of oligothiophenes and their utilization as fluorescent ligands for spectral assignment of protein aggregates. *Org. Biomol. Chem. 9*, 8356−8370.

(13) Nilsson, K. P., Aslund, A., Berg, I., Nystrom, S., Konradsson, P., Herland, A., Inganas, O., Stabo-Eeg, F., Lindgren, M., Westermark, G. T., Lannfelt, L., Nilsson, L. N., and Hammarstrom, P. (2007) Imaging distinct conformational states of amyloid-beta fibrils in Alzheimer's disease using novel luminescent probes. *ACS Chem. Biol. 2*, 553−560.

(14) Lord, A., Philipson, O., Klingstedt, T., Westermark, G., Hammarstrom, P., Nilsson, K. P., and Nilsson, L. N. (2011) Observations in APP bitransgenic mice suggest that diffuse and compact plaques form via independent processes in Alzheimer's disease. *Am. J. Pathol. 178*, 2286−2298.

(15) Hoyer, W., Gronwall, C., Jonsson, A., Stahl, S., and Hard, T. (2008) Stabilization of a beta-hairpin in monomeric Alzheimer's amyloid-beta peptide inhibits amyloid formation. *Proc. Natl. Acad. Sci. U.S.A. 105*, 5099−5104.

(16) Sturchler-Pierrat, C., Abramowski, D., Duke, M., Wiederhold, K. H., Mistl, C., Rothacher, S., Ledermann, B., Burki, K., Frey, P., Paganetti, P. A., Waridel, C., Calhoun, M. E., Jucker, M., Probst, A., Staufenbiel, M., and Sommer, B. (1997) Two amyloid precursor protein transgenic mouse models with Alzheimer disease-like pathology. *Proc. Natl. Acad. Sci. U.S.A. 94*, 13287−13292.

(17) Jin, L. W., Claborn, K. A., Kurimoto, M., Geday, M. A., Maezawa, I., Sohraby, F., Estrada, M., Kaminksy, W., and Kahr, B. (2003) Imaging linear birefringence and dichroism in cerebral amyloid pathologies. *Proc. Natl. Acad. Sci. U.S.A. 100*, 15294−15298.

(18) Ellingsen, P. G., Reitan, N. K., Pedersen, B. D., and Lindgren, M. (2013) Hyperspectral analysis using the correlation between image and reference. *J. Biomed. Opt. 18*, 20501.

(19) Wegenast-Braun, B. M., Skodras, A., Bayraktar, G., Mahler, J., Fritschi, S. K., Klingstedt, T., Mason, J. J., Hammarstrom, P., Nilsson, K. P., Liebig, C., and Jucker, M. (2012) Spectral discrimination of cerebral amyloid lesions after peripheral application of luminescent conjugated oligothiophenes. *Am. J. Pathol. 181*, 1953−1960.

(20) Mathis, C. A., Wang, Y., Holt, D. P., Huang, G. F., Debnath, M. L., and Klunk, W. E. (2003) Synthesis and evaluation of 11C-labeled 6-substituted 2-arylbenzothiazoles as amyloid imaging agents. *J. Med. Chem. 46*, 2740−2754.

(21) Oddo, S., Caccamo, A., Tran, L., Lambert, M. P., Glabe, C. G., Klein, W. L., and LaFerla, F. M. (2006) Temporal profile of amyloid-beta (Abeta) oligomerization in an *in vivo* model of Alzheimer disease. A link between Abeta and tau pathology. *J. Biol. Chem. 281*, 1599−1604.

(22) Vom Berg, J., Prokop, S., Miller, K. R., Obst, J., Kalin, R. E., Lopategui-Cabezas, I., Wegner, A., Mair, F., Schipke, C. G., Peters, O., Winter, Y., Becher, B., and Heppner, F. L. (2012) Inhibition of IL-12/IL-23 signaling reduces Alzheimer's disease-like pathology and cognitive decline. *Nat. Med. 18*, 1812−1819.

(23) Gengler, S., Hamilton, A., and Holscher, C. (2010) Synaptic plasticity in the hippocampus of a APP/PS1 mouse model of Alzheimer's disease is impaired in old but not young mice. *PLoS One 5*, e9764.

(24) Bittner, T., Burgold, S., Dorostkar, M. M., Fuhrmann, M., Wegenast-Braun, B. M., Schmidt, B., Kretzschmar, H., and Herms, J. (2012) Amyloid plaque formation precedes dendritic spine loss. *Acta Neuropathol. 124*, 797−807.

(25) Citron, M. (2010) Alzheimer's disease: strategies for disease modification. *Nat Rev. Drug Discovery 9*, 387−398.

(26) Grathwohl, S. A., Kalin, R. E., Bolmont, T., Prokop, S., Winkelmann, G., Kaeser, S. A., Odenthal, J., Radde, R., Eldh, T., Gandy, S., Aguzzi, A., Staufenbiel, M., Mathews, P. M., Wolburg, H., Heppner, F. L., and Jucker, M. (2009) Formation and maintenance of Alzheimer's disease beta-amyloid plaques in the absence of microglia. *Nat. Neurosci. 12*, 1361−1363.

(27) Meyer-Luehmann, M., Coomaraswamy, J., Bolmont, T., Kaeser, S., Schaefer, C., Kilger, E., Neuenschwander, A., Abramowski, D., Frey, P., Jaton, A. L., Vigouret, J. M., Paganetti, P., Walsh, D. M., Mathews, P. M., Ghiso, J., Staufenbiel, M., Walker, L. C., and Jucker, M. (2006) Exogenous induction of cerebral beta-amyloidogenesis is governed by agent and host. *Science 313*, 1781−1784.

(28) Frost, B., and Diamond, M. I. (2010) Prion-like mechanisms in neurodegenerative diseases. *Nat. Rev. Neurosci. 11*, 155−159.

(29) Zetterberg, H., and Blennow, K. (2012) Biomarker evidence for uncoupling of amyloid build-up and toxicity in Alzheimer's disease. *Alzheimer's Dementia*, DOI: 10.1016/j.jalz.2012.07.002.